



 Cite this: *RSC Adv.*, 2021, 11, 18387

Improved energy storage performance of PbZrO₃ antiferroelectric thin films crystallized by microwave radiation

 Yin Fang, Yu Bai, Yi Zhuo Li, Ning Liu, Fan Zhang, Chao Wang and Zhan Jie Wang *

Energy storage dielectric capacitors based on a physical charge-displacement mechanism have attracted much attention due to their high power density and fast charge-discharge characteristics. How to improve the energy storage capacity of dielectric materials has become an important emerging research topic. Here, antiferroelectric PbZrO₃ films were prepared by chemical solution deposition on Pt/Ti/SiO₂/Si substrates and crystallized by microwave radiation. The effects of microwave radiation on the antiferroelectric properties and energy storage performance were investigated. In contrast to ordinary heating, microwave radiation can crystallize the amorphous PbZrO₃ films into the perovskite phase at 750 °C in only 180 seconds. The PbZrO₃ films have a highly (100)-preferred orientation and dense microstructure, which is beneficial to enhance the stability of antiferroelectric phase and the electric breakdown strength. The PbZrO₃ films show a recoverable energy storage density of 14.8 J cm⁻³ at 740 kV cm⁻¹, which is approximately 40% higher than that of the PbZrO₃ films crystallized by ordinary heating. The results reveal that microwave radiation is an effective method to improve energy storage performance of antiferroelectric films.

Received 13th February 2021

Accepted 12th May 2021

DOI: 10.1039/d1ra01203g

rsc.li/rsc-advances

1. Introduction

Energy storage dielectric capacitors made of dielectric materials have attracted extensive attention due to their high power density and fast charge-discharge characteristics, which have promising applications in pulsed electronic systems.¹⁻⁵ As a typical dielectric material, PbZrO₃ (PZO)-based antiferroelectric (AFE) films have been widely studied for energy storage because of the higher energy storage density achieved during the electric-field-induced antiferroelectric-ferroelectric (AFE-FE) phase transition.⁶⁻⁹ As given in Fig. 1, the recoverable energy storage density (W_{rec}) can be presented by integrating the area between the polarization-electric field (P - E) hysteresis loop and the polarization axis, and the consumed energy density (W_{loss}) can be calculated from the enclosed area of the hysteresis loop. The η is the ratio of W_{rec} to $W_{\text{rec}} + W_{\text{loss}}$, which is mainly affected by the transition behavior between the AFE and FE phases. Therefore, improving the maximum polarization (P_{max}) as high as the value of theory, increasing electric breakdown strength (E_{BDS}), and making the AFE phase stable ($E_{\text{A-F}}$ and $E_{\text{F-A}}$) are three main methods to enhance the W_{rec} . For instance, the large W_{rec} in AFE PZO films could be achieved by adding gold nanoparticles to increase of maximum polarization.¹⁰ By doping La³⁺, Ca²⁺ and Sr²⁺ with smaller ionic radius than that of Pb²⁺ can make the AFE phase stable, so as to improve the W_{rec} .^{8,11-14} An

enhanced W_{rec} and reduced W_{loss} were obtained in Eu-doped PZO AFE films because of the easier domain motion caused by the introduction of Pb vacancies due to the donor effect of Eu.¹⁵ Moreover, controlling the crystalline preferred orientation, which may increase the maximum polarization and the stability of AFE phase, is an effective way to improve the W_{rec} .¹⁶⁻¹⁸ Besides, the W_{rec} of AFE films can also be improved by using special preparation methods and adjusting process parameters to obtain high-quality films.¹⁹⁻²³ For example, an improved W_{rec} of AFE films was obtained by modifying chemical solution with

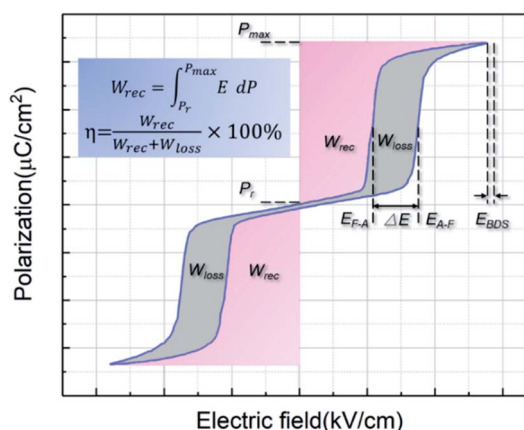


Fig. 1 A schematic diagram for the energy storage of AFE materials.

School of Materials Science and Engineering, Shenyang University of Technology, Shenyang 110870, China. E-mail: wangzj@imr.ac.cn; wangzhanjie@sut.edu.cn



polyvinylpyrrolidone (PVP), which is due to the reduction of cracks in the films.²¹ By controlling the deposition temperature in the process of pulsed laser deposition, the AFE films could be made more compact and form a more stable AFE phase, thus improving the W_{rec} .²²

Recently, microwave radiation has been widely applied to crystallize functional film materials.^{24–29} Compared to ordinary heating, microwave radiation could achieve perovskite $\text{Pb}(\text{Zr},\text{Ti})\text{O}_3$ (PZT) films with good ferroelectric properties in a short-time or at low-temperatures, because it could reduce the potential barrier of phase transition from amorphous to perovskite phase during the crystallization process.^{24–26} Moreover, microwave radiation can change the microstructure and density of the ferroelectric films, because the crystallization process (the nucleation and growth of perovskite grains) under microwave radiation is different from that of ordinary heating.^{25,28} At present, the crystallization process of AFE thin films under microwave radiation has not been reported. However, according to the research results of ferroelectric thin films, microwave radiation may be used to control the microstructure of AFE films, increase the electric breakdown strength and the stability of AFE phase, thus performing a better energy storage performance. In addition, microwave radiation annealing is expected to be an energy-saving and environment-friendly process for the preparation of AFE films due to its short time or low temperature.

In this work, we prepared the amorphous PZO films by chemical solution deposition and then crystallized the films by microwave radiation. The AFE properties and energy storage performance of PZO films were investigated. The PZO films processed by microwave radiation for only 180 seconds have a dense microstructure, and show a highly (100)-preferred orientation. Compared with the conventional annealed PZO thin films, the microwave irradiated PZO films have a higher AFE phase stability and electric breakdown strength, and a lower remanent polarization. It is found that the W_{rec} of the PZO films crystallized by microwave radiation is 14.8 J cm^{-3} at 740 kV cm^{-1} , which is 40% higher than that of the PZO films crystallized by ordinary heating. Our results demonstrate that using microwave radiation in the crystallization of AFE thin films is an effective method to improve their energy storage performance.

2. Experimental details

The amorphous PZO films were fabricated on $\text{Pt}/\text{Ti}/\text{SiO}_2/\text{Si}$ substrates by chemical solution deposition. Lead acetate trihydrate ($\text{Pb}(\text{CH}_3\text{COO})_2 \cdot 3\text{H}_2\text{O}$) and zirconium-*n*-propoxide ($\text{Zr}(\text{OCH}_2\text{CH}_2\text{CH}_3)_4$) were used as starting raw materials to prepare PZO precursor solution. Lead acetate trihydrate ($\text{Pb}(\text{CH}_3\text{COO})_2 \cdot 3\text{H}_2\text{O}$) was dissolved in 2-methoxyethanol at $130 \text{ }^\circ\text{C}$ for 90 minutes. A 20 mol%-excessive lead was added to the solution as a compensation for lead loss. After cooling to room temperature, zirconium-*n*-propoxide ($\text{Zr}(\text{OCH}_2\text{CH}_2\text{CH}_3)_4$) was mixed into the above solution and stirred for 120 minutes. After aging for 24 hours, the concentration of the final PZO precursor solution was 0.5 mol L^{-1} . The PZO precursor was

deposited on the $\text{Pt}/\text{Ti}/\text{SiO}_2/\text{Si}$ substrates by using a spin coater with a spin speed of 3000 rpm for 40 seconds. The coated films were dried on a heat plate at $120 \text{ }^\circ\text{C}$ for 5 minutes and then pyrolyzed at $450 \text{ }^\circ\text{C}$ for 5 minutes. After repeating the steps above five times, the PZO thin films with the designed thickness were obtained. To prevent the loss of Pb during the final heat treatment, 0.4 mol L^{-1} PbO precursor was deposited on these PZO thin films with the same process above as a capping layer. Finally, the amorphous PZO films were processed by microwave radiation at $750 \text{ }^\circ\text{C}$ for 60, 120 and 180 seconds of total treatment, respectively. As a comparison, the amorphous PZO films were also crystallized by ordinary heating, that is, the amorphous PZO films were heated in an electric furnace at $750 \text{ }^\circ\text{C}$ for 30 minutes. The heating rate in the ordinary heating process was about $30 \text{ }^\circ\text{C min}^{-1}$.

The microwave radiation equipment used in this study is the TE_{103} mode with a frequency of 2.45 GHz and the standing wave with a wavelength of 14.8 cm can be modulated in the waveguide. The microwave electric field or microwave magnetic fields can be adjusted to the maximum at the position of the sample. In this study, all samples were irradiated in the maximum magnetic field. The elevated temperature of the sample during the microwave radiation processing was measured by using a noncontact infrared thermometer (CTLaser2M; Optris, Berlin, Germany). Fig. 2 presents a typical temperature-rising curve of $\text{PZO}/\text{Pt}/\text{Ti}/\text{SiO}_2/\text{Si}$ sample during microwave radiation at the out power of 600 W. The heating rate and the maximum temperature were controlled to be $50 \text{ }^\circ\text{C s}^{-1}$ and $750 \text{ }^\circ\text{C}$ by tuning the out power. The inset is the schematic of samples irradiated in the microwave magnetic field.

The phase composition and orientation of the PZO films were analyzed by X-ray diffraction (XRD; Discover 8, $\text{CuK}\alpha$ radiation, Bruker, Germany). The scanning electron microscopy (FE-SEM; SU8010N, Hitachi, Japan) was used to observe the surface and cross-sectional morphologies. The microstructure was investigated by transmission electron microscopy (TEM; Tecnai G2 F20, FEI, Eindhoven, the Netherlands). The polarization–electric field (P – E) hysteresis loops and leakage current

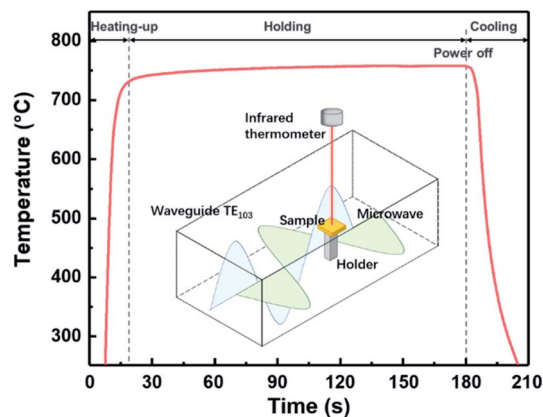


Fig. 2 The heating curve of PZO films by microwave radiation. Inset is a schematic diagram for the equipment of microwave radiation and temperature measurement.

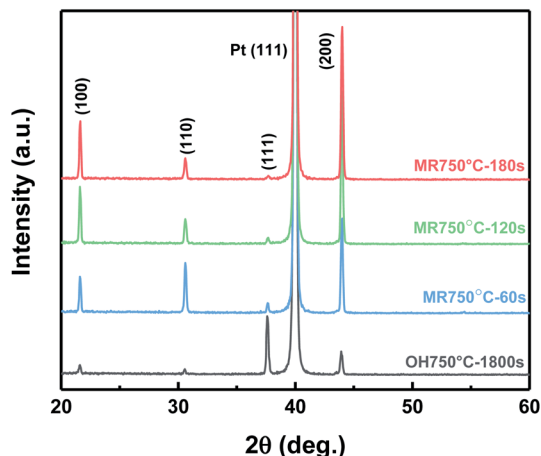


Fig. 3 The XRD patterns of PZO films crystallized by ordinary heating (OH) and microwave radiation (MR).

density of the PZO films were measured at 1 kHz at room temperature by using a standard ferroelectric testing system (TF2000E; Aixacct, Aachen, Germany).

3. Results and discussions

Fig. 3 presents the XRD patterns of PZO films processed by microwave radiation for different times, which shows all the

films crystallized into the perovskite phase, and no secondary phase is detected. As the microwave radiation time was 60 seconds, the diffraction peaks of perovskite phase are randomly oriented. When the microwave radiation time was increased to 120 seconds, the diffraction intensity of (111) planes decreased, while the diffraction intensity of (100) and (200) planes rapidly increased. With further raising the time to 180 seconds, the diffraction intensity remained almost unchanged, meaning that PZO films have been completely crystallized into the perovskite phase by microwave radiation for 180 seconds. The (100)-orientated degree can be calculated by $I_{(100)}/(I_{(100)} + I_{(110)} + I_{(111)})$, where I corresponds the intensity of the peaks. For the PZO films processed by microwave radiation for 180 seconds, the (100)-orientated degree is 80%, thus the PZO films show a highly (100)-preferred orientation. For comparison, the XRD pattern of PZO films processed by ordinary heating is also given in Fig. 3. The PZO films annealed for 30 minutes crystallized into the perovskite phase, but a (111)-orientated degree of 82% was obtained, which means the PZO films show a highly (111)-preferred orientation. It is a common result for the PZO films on the Pt/Ti/SiO₂/Si substrate crystallized by ordinary heating.¹⁰ In contrast, the perovskite PZO films can be obtained by microwave radiation in only 3 minutes, and have a stronger peak intensity of perovskite phase, which means that a higher crystallization quality is achieved in the microwave-irradiated film.

The surface and cross-sectional morphologies of the PZO films processed by microwave radiation for different times are

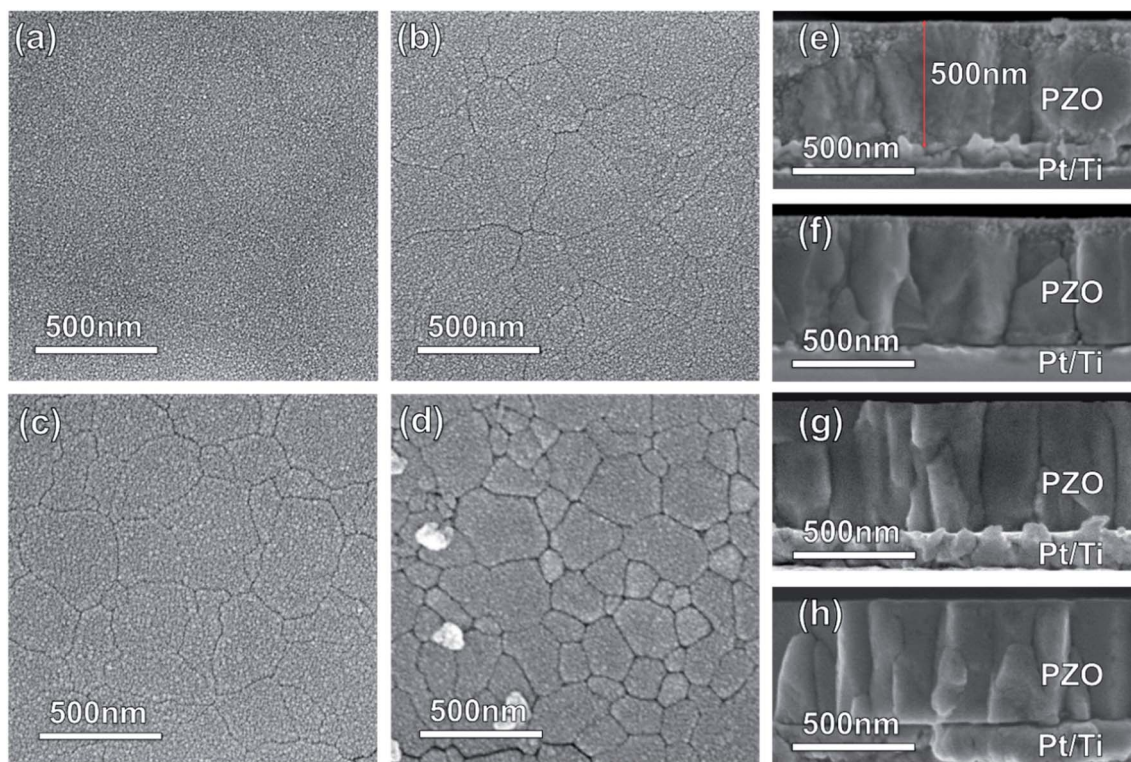


Fig. 4 The surface SEM images for the PZO films processed by microwave radiation for (a) 60, (b) 120, (c) 180 seconds and (d) ordinary heating for 1800 seconds. The cross-sectional SEM images for the PZO films processed by microwave radiation for (e) 60, (f) 120, (g) 180 seconds and (h) ordinary heating for 1800 seconds.

shown in Fig. 4. Cross-sectional SEM images show that the thickness of PZO films is all about 500 nm, and a columnar grain structure can be observed. As shown in Fig. 4(a), the PZO film processed by microwave radiation for 60 seconds shows a featureless microstructure. From the cross-sectional morphology (Fig. 4(e)), it can be seen that fine grains are distributed on the film surface. When the microwave radiation time was increased to 120 seconds, large grains appeared on the film surface (Fig. 4(b)), but some regions containing the fine grains can also be observed (Fig. 4(f)). When the time was further increased to 180 seconds, the large grains filled the whole film surface (Fig. 4(c)), and the PZO film has a columnar grain structure throughout the whole thickness of the film (Fig. 4(g)). As mentioned above, the XRD results for the PZO films processed by microwave radiation for different times show that the films are composed of perovskite phase, and no second phase is detected. Therefore, the large grains can be considered as the perovskite phase, while the fine grains may be the pyrochlore phase, which cannot be detected by XRD due to its small quantity. To clarify this point, we have also done TEM studies, and confirmed that the fine grains are the pyrochlore phase, which will be discussed below. Fig. 4(d) and (h) show the surface and cross-sectional morphologies of the PZO film crystallized by ordinary heating. The PZO film also has a columnar grain structure of the perovskite phase throughout the whole thickness of the film. In contrast, the PZO film crystallized by microwave radiation for 180 seconds (Fig. 4(c)) shows a smoother surface and denser microstructure. It will be beneficial to reduce the leakage current density of the PZO film and then improve the electric breakdown strength.³⁰

Fig. 5 shows cross-sectional TEM images of the PZO film processed by microwave radiation for 120 and 180 seconds. As presented in Fig. 5(a), when the microwave radiation time was 120 seconds, the film has a columnar grain structure, and the columnar perovskite grains have grown almost to the surface of

the film. However, some regions containing fine grains could also be observed on the surface of the film. Fig. 5(b) shows selected-area electron diffraction patterns for the fine grains region marked with the circle in Fig. 5(a). The diffraction ring patterns indicate that the fine grains belong to the pyrochlore phase. This result is in good agreement with that observed by SEM. As shown in Fig. 5(c), when the microwave radiation time was increased to 180 seconds, the columnar perovskite grains have grown throughout the whole film, and no region containing fine grains can be observed, showing that the film has been crystallized into the perovskite phase completely. Fig. 5(d) shows a HRTEM image on the PZO/Pt interface, indicating that the (100) plane of the perovskite grain is parallel to the (111) plane of Pt, thereby the perovskite grains have [001]-crystal orientation in the out-of-plane direction. This can also be proved by the fast Fourier transform (FFT) patterns transformed from the HRTEM image of Fig. 5(d), as shown as the inset in Fig. 5(d). Based on the above results of XRD, SEM and TEM, it can be concluded that the perovskite PZO films with a dense microstructure can be obtained by microwave radiation in a short time, and have a highly (100)-preferred orientation.

The rapid crystallization of PZO thin films under microwave radiation may be caused by several factors. It has been reported that amorphous oxide films on the Pt/Ti/SiO₂/Si substrate, such as PZT, LaNiO₃ and PbTiO₃ films, can be crystallized into the perovskite phase in a short time by microwave radiation because the crystallization process under microwave radiation is different from the conventional crystallization process.^{26,28,31} In the process of microwave radiation, the heat mainly comes from the interaction between bottom electrode and silicon substrate and microwave.³² Therefore, the heat flows from the film/substrate interface to the film surface during the microwave radiation process. The directional heat flux in the films is different from that in the conventional annealed films, which possibly affects the process of nucleation and growth of perovskite grains in PZO films, thus changing the nucleation and growth rates and preferred orientation. In addition, it can be seen from Fig. 2 that the heating rate of the sample in the microwave radiation process was about 50 °C s⁻¹, which is much faster than that in the ordinary heating, and is fast as that in rapid thermal annealing (RTA) process. The crystallization of FE and AFE thin films by RTA has been widely studied, and it is clear that the rapid heating rate can promote the phase transition from amorphous to perovskite.^{12,33–36} In addition to the above microwave thermal effect, the “nonthermal effect” of microwave should be considered in the process of microwave radiation. It has been reported that in the microwave radiation process, the electromagnetic energy of microwave can reduce the activation energy required for the phase transition from amorphous phase to perovskite phase of ferroelectric thin films during the crystallization process, so that the nucleation and growth of perovskite grains are easier.^{25,28} Moreover, according to the ponderomotive force (PMF) model, when there is a concentration gradient of charged ions at the grain boundary or interface, microwave can enhance the transport of these charged ions.³⁷ Therefore, in the crystallization process of PZO films, microwave radiation can not only induce the nucleation

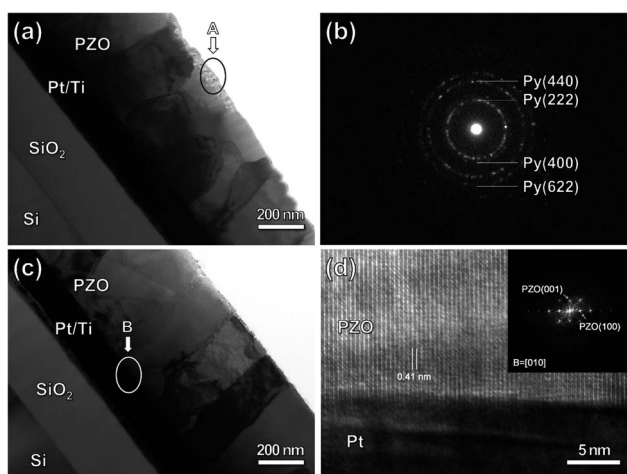


Fig. 5 (a) A cross-sectional TEM image for the PZO films processed by microwave radiation for 120 seconds, and (b) selected-area diffraction patterns for the area as shown in (a), (c) a cross-sectional TEM image for the PZO films processed by microwave radiation for 180 seconds, and (d) a HRTEM image for the area as shown in (c).

but also promote the growth of perovskite grains. In addition, microwave radiation seems to be beneficial to the directional growth of perovskite grains. The effect of microwave radiation on the orientation of LNO films has been investigated by Zhu *et al.*,³¹ and they found that the (100)-oriented LNO films could be obtained through microwave radiation, while (110)-orientation predominated in the films prepared by ordinary heating. In this study, the PZO films crystallized by microwave radiation show a highly (100)-preferred orientation, while those crystallized by ordinary heating show a highly (111)-preferred orientation. To sum up, the crystallization process of AFE PZO thin films under microwave radiation is different from the conventional crystallization process, and the rapid crystallization of PZO thin films is the result of the above factors. The perovskite PZO thin films with dense microstructure and highly (100)-preferred orientation will be expected to have good energy storage performance.

Fig. 6(a) shows the leakage current characteristics of the PZO films processed by microwave radiation for 180 seconds and ordinary heating. The leakage current density of PZO film crystallized by microwave radiation is reduced by one order of magnitude compared with that of ordinary heating. The reduced leakage current density of PZO film crystallized by microwave radiation is attributed to the smoother surface and denser microstructure. Generally, the leakage current density has a significant influence on the E_{BDS} of dielectric capacitors.^{20,35} The E_{BDS} can be analyzed by the Weibull distribution function, and calculated by the following formula:³⁶

$$X_i = \ln(E_i)$$

$$Y_i = \ln\left(\ln\left(\frac{1}{1 - P_i}\right)\right)$$

$$P_i = \frac{i}{n + 1}$$

where E_i is the E_{BDS} of each sample, i is serial number of samples and n is the total number of samples. P_i is the probability of sample breakdown. The mean E_{BDS} can be extracted from the fitting line of X_i and Y_i , which is the intercept on the axis of $Y_i = 0$. The scatter and reliability of E_{BDS} can be evaluated according to the shape parameter (β), which is the slope of the fitting line. As shown in Fig. 6(b), the E_{BDS} of PZO films crystallized by microwave radiation is 764 kV cm^{-1} , which is larger than that of PZO films crystallized by ordinary heating (558 kV cm^{-1}). Moreover, the films crystallized by microwave radiation have a larger β value (37.87), indicating that the E_{BDS} has less scatter and higher reliability. These results are attributed to the fact that the microstructure of PZO films becomes more compact after 180 seconds of microwave radiation, which reduces the leakage current density. Therefore, the E_{BDS} of PZO films can be improved by microwave radiation during the crystallization process.

The polarization–electric field (P – E) hysteresis loops of the PZO films processed by microwave radiation for 180 seconds and ordinary heating are shown Fig. 7(a) and (c). Both show a clear double hysteresis loop with antiferroelectric characteristics. Compared with the PZO films crystallized by ordinary heating, the films crystallized by microwave radiation show a significant decrease of the remanent polarization (1.6 $\mu\text{C cm}^{-2}$), which is related to the high crystallization quality. Moreover, a clear difference in the switching field between AFE and FE phases can be observed. The magnitude of switching fields could be obtained from the peaks of displacement current in the current vs. electric field curves (Fig. 7(b) and (d)). In the PZO films crystallized by microwave radiation, the $E_{\text{A-F}}$ and $E_{\text{F-A}}$ are 498 kV cm^{-1} and 274 kV cm^{-1} , respectively, which are much larger than those of the PZO films crystallized by ordinary heating, implying that the AFE phase becomes more stable in the microwave-irradiated PZO films. The stability of AFE phase may be related to the preferred orientation of the films except the high crystallization quality. As mentioned above, XRD study indicates that the PZO films crystallized by microwave radiation have the highly (100)-preferred orientation, while the PZO films

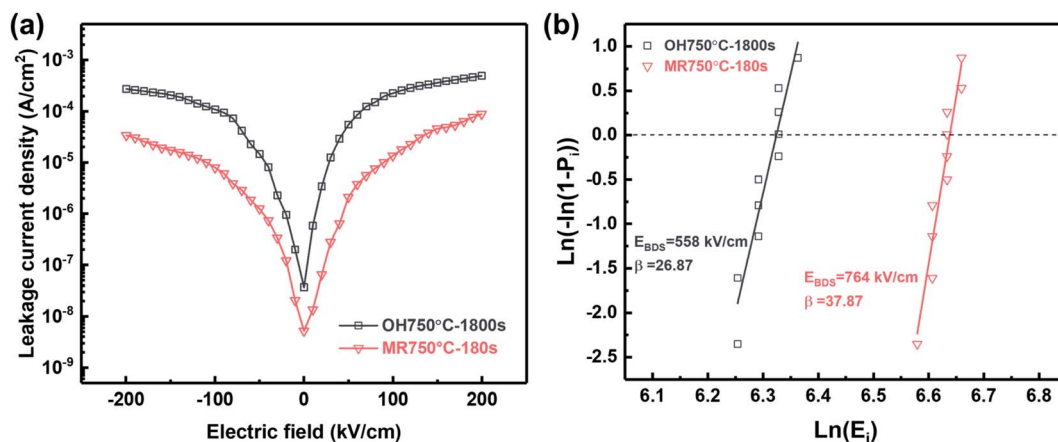


Fig. 6 (a) Leakage current density versus electric field of the PZO films processed by microwave radiation (MR) for 180 seconds and ordinary heating (OH). (b) Weibull plot of the E_{BDS} of the PZO films processed by microwave radiation for 180 seconds and ordinary heating.

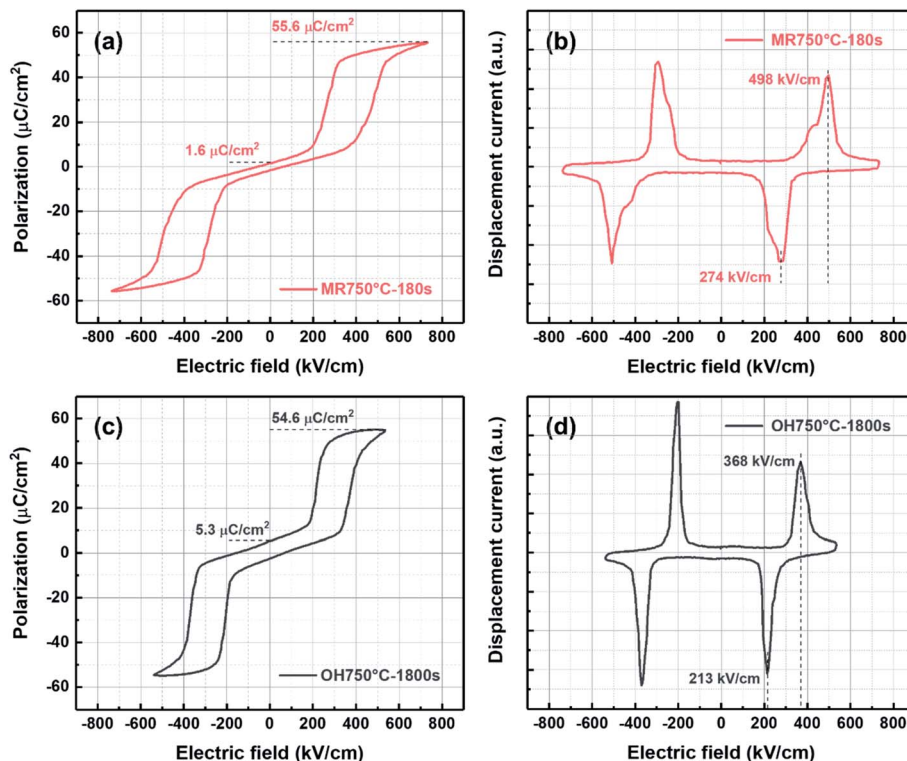


Fig. 7 P - E hysteresis loops of PZO films processed by (a) microwave radiation (MR) for 180 seconds and (c) ordinary heating (OH). Displacement current measured from P - E loops of PZO films processed by (b) microwave radiation for 180 seconds and (d) ordinary heating.

crystallized by ordinary heating have a highly (111)-preferred orientation. Zhai *et al.*³⁸ have studied the orientation-dependent phase switching process of PZO-based AFE thin films on the Pt/Ti/SiO₂/Si substrate. They found that the (111)-oriented films deposited on the Pt/Ti/SiO₂/Si substrate showed a smaller field-induced phase switching as compared to the (100)-preferred films deposited on the LaNiO₃-buffered Pt/Ti/SiO₂/Si substrate. Similar results have been reported by Hao *et al.*³⁹ For the PZO films with the (100)-preferred orientation, the angle between the directions of applied electric field and [111] polar axis of the rhombohedral phase is higher than that of the PZO films with the (111)-preferred orientation.⁴⁰ Consequently, more energy is

needed to arrange the dipoles in the direction of electric field for the (100)-oriented PZO films, that is, the higher the orientation factor along the (100) direction, the more stable the AFE phase is.

According to Fig. 7(a) and (c), the energy storage density (W_{rec}) and efficiency (η) for the PZO films crystallized by microwave radiation and ordinary heating were calculated, respectively. As shown in Fig. 8(a), the W_{rec} increased with increasing applied electric field. In low electric fields, the PZO thin films annealed by ordinary heating show higher W_{rec} , because the switching field between AFE and FE phases is lower. However, due to the high E_{BDS} of the PZO films crystallized by

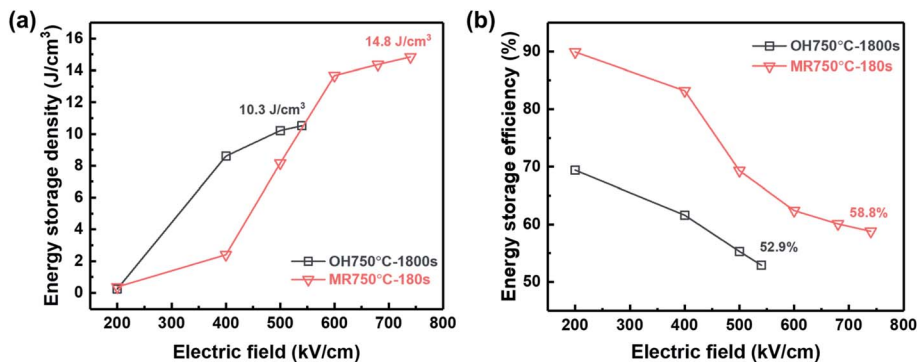


Fig. 8 The (a) recoverable energy storage density and (b) energy storage efficiency of PZO films processed by microwave radiation for (MR) 180 seconds and ordinary heating (OH) at different applied electric field.

Comparison of performance of the PZO films crystallized by MR and OH

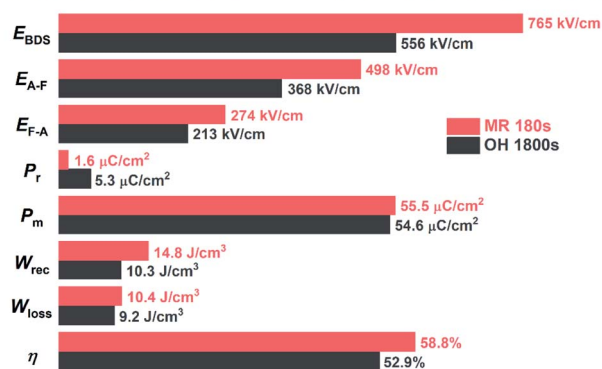


Fig. 9 The differences in various parameters of PZO films crystallized by microwave radiation (MR) and ordinary heating (OH).

microwave radiation, the maximum W_{rec} of 14.8 J cm^{-3} is achieved at 740 kV cm^{-1} , which is approximately 40% higher than that of the PZO films crystallized by ordinary heating. As given in Fig. 8(b), the η of the PZO films crystallized by microwave radiation is also higher than that of the PZO films crystallized by ordinary heating. Fig. 9 summarizes the differences in various parameters of PZO films crystallized by microwave radiation and ordinary heating, showing the main influence factors on energy storage performance. As shown in Fig. 9, the PZO films crystallized by microwave radiation and ordinary heating show approximate values of energy loss, which are 10.4 and 9.2 J cm^{-3} , respectively, due to the simultaneous increase E_{A-F} and E_{F-A} . Apparently, the significant improvement in the energy storage density and efficiency of PZO films crystallized by microwave radiation is mainly attributed to the increase of the E_{BDS} , the increase of AFE phase stability and the decrease of remanent polarization. The results demonstrate that the energy storage density and efficiency of AFE films could be improved effectively by microwave radiation during the crystallization process.

Fig. 10 summarizes the energy storage properties of PZO films prepared by different methods reported in the literature. By using pulsed laser deposition (PLD) and magnetron sputtering, high-quality PZO films with a higher η , but W_{rec} is relatively lower.^{16,40–42} In the chemical deposition method, although perovskite PZO films can also be obtained by rapid thermal annealing (RTA),^{8,12,43} the PZO films crystallized by microwave radiation have larger W_{rec} and η . Our results demonstrate that using microwave radiation in the crystallization of AFE thin films is an effective method to improve their energy storage performance. At present, the research works are mainly focused on improving the energy storage performance of AFE thin films by doping, compounding and other methods.^{10–14} Although the research object of this study is pure PZO thin films, it can be conceivable that microwave radiation can also be used for the preparation of doped or composite AFE thin films to further improve the energy storage properties of these films.

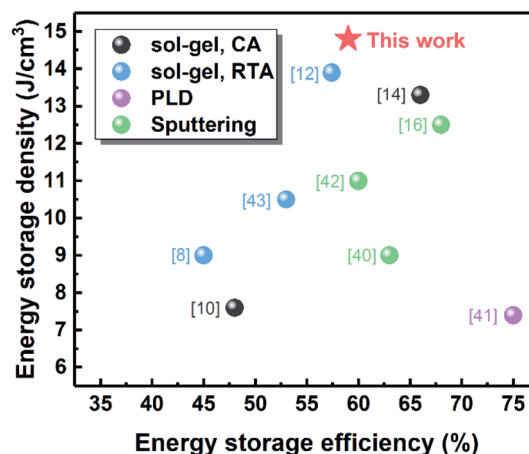


Fig. 10 Summary of reported data on energy storage density and efficiency of PZO films obtained from different preparation methods.

4. Conclusion

In this work, PZO films were prepared by chemical solution deposition and then crystallized by microwave radiation. The PZO films processed by microwave radiation for only 180 seconds have the dense microstructure with a highly (100)-preferred orientation. It is found that the W_{rec} of the PZO films crystallized by microwave radiation is 14.8 J cm^{-3} at 740 kV cm^{-1} , which is 40% higher than that of the PZO films crystallized by ordinary heating. The improvement of energy storage performance is attributed to the increase of AFE phase stability and electric breakdown strength, and decrease of remanent polarization. Our results demonstrate that using microwave radiation in the crystallization of AFE thin films is an effective method to improve their energy storage performance.

Conflicts of interest

There are no conflicts of interest to declare.

Acknowledgements

This work was supported by the National Natural Science Foundation of China (No. 51902210), the Regional Innovation and Development Joint Fund Project of Natural Science Foundation of Liaoning Province in 2020 (No. 2020-YKLH-23) and the Central Government Guiding Local Science and Technology Development Funds of Liaoning Province in 2021 (No. 2021JH6/10500168).

References

- Z. Sun, Z. Wang, Y. Tian, G. Wang, W. Wang, M. Yang, X. Wang, F. Zhang and Y. Pu, *Adv. Electron. Mater.*, 2020, **6**, 1900698.
- B. L. Phoon, C. W. Lai, J. C. Juan, P. L. Show and W. H. Chen, *Int. J. Energy Res.*, 2019, **43**, 5151–5174.

- 3 H. Qi, R. Zuo, A. Xie, J. Fu and D. Zhang, *J. Eur. Ceram. Soc.*, 2019, **39**, 3703–3709.
- 4 L. Zhao, Q. Liu, J. Gao, S. Zhang and J. F. Li, *Adv. Mater.*, 2017, **29**, 1701824.
- 5 B. Xu, J. Íñiguez and L. Bellaiche, *Nat. Commun.*, 2017, **8**, 15682.
- 6 H. Wang, Y. Liu, T. Yang and S. Zhang, *Adv. Funct. Mater.*, 2019, **29**, 1807321.
- 7 X. Liu, Y. Li and X. Hao, *J. Mater. Chem. A*, 2019, **7**, 11858–11866.
- 8 T. Zhang, Y. Zhao, W. Li and W. Fei, *Energy Storage Mater.*, 2019, **18**, 238–245.
- 9 Z. Lin, Y. Chen, Z. Liu, G. Wang, D. Rémiens and X. Dong, *J. Eur. Ceram. Soc.*, 2018, **38**, 3177–3181.
- 10 Y. Z. Li, Z. J. Wang, Y. Bai, W. Liu and Z. D. Zhang, *J. Am. Ceram. Soc.*, 2019, **102**, 5253–5261.
- 11 S. Li, H. Nie, G. Wang, C. Xu, N. Liu, M. Zhou, F. Cao and X. Dong, *J. Mater. Chem. C*, 2019, **7**, 1551–1560.
- 12 Y. Z. Li, Z. J. Wang, Y. Bai and Z. D. Zhang, *J. Eur. Ceram. Soc.*, 2020, **40**, 1285–1292.
- 13 J. Gao, Y. Zhang, L. Zhao, K. Y. Lee, Q. Liu, A. Studer, M. Hinterstein, S. Zhang and J. F. Li, *J. Mater. Chem. A*, 2019, **7**, 2225–2232.
- 14 X. Hao, J. Zhai and X. Yao, *J. Am. Ceram. Soc.*, 2009, **92**, 1133–1135.
- 15 M. Ye, Q. Sun, X. Chen, Z. Jiang and F. Wang, *J. Am. Ceram. Soc.*, 2011, **94**, 3234–3236.
- 16 J. Ge, D. Remiens, X. Dong, Y. Chen, J. Costecalde, F. Gao, F. Cao and G. Wang, *Appl. Phys. Lett.*, 2014, **105**, 112908.
- 17 X. Hao, J. Zhou and S. An, *J. Am. Ceram. Soc.*, 2011, **94**, 1647–1650.
- 18 M. D. Nguyen, T. T. Trinh, H. T. Dang and H. N. Vu, *Thin Solid Films*, 2020, **697**, 137794.
- 19 Y. Liu, X. Hao, J. Zhou, J. Xu and S. An, *J. Alloys Compd.*, 2011, **509**, 8779–8782.
- 20 Y. Liu, Y. Wang, X. Hao and J. Xu, *Ceram. Int.*, 2013, **39**, S513–S516.
- 21 Y. Wang, X. Hao, J. Yang, J. Xu and D. Zhao, *J. Appl. Phys.*, 2012, **112**, 034105.
- 22 M. D. Nguyen and G. Rijnders, *J. Eur. Ceram. Soc.*, 2018, **38**, 4953–4961.
- 23 L. Zhang, M. Liu, W. Ren, Z. Zhou, G. Dong, Y. Zhang, B. Peng, X. Hao, C. Wang, Z. De Jiang, W. Jing and Z. G. Ye, *RSC Adv.*, 2017, **7**, 8388–8393.
- 24 Z. Wang, Y. Chen, Y. Otsuka, M. Zhu, Z. Cao and H. Kokawa, *J. Am. Ceram. Soc.*, 2011, **94**, 404–409.
- 25 Y. N. Chen, Z. J. Wang, T. Yang and Z. D. Zhang, *Acta Mater.*, 2014, **71**, 1–10.
- 26 Y. N. Chen and Z. J. Wang, *J. Am. Ceram. Soc.*, 2013, **96**, 90–95.
- 27 Y. J. Zhang, Z. J. Wang, Y. Bai, Y. Z. Li, W. Liu and Z. D. Zhang, *J. Alloys Compd.*, 2018, **757**, 24–30.
- 28 Y. J. Zhang, Z. J. Wang, Y. N. Chen and Z. D. Zhang, *J. Eur. Ceram. Soc.*, 2018, **38**, 105–111.
- 29 H. J. Han, Y. N. Chen and Z. J. Wang, *RSC Adv.*, 2015, **5**, 92940–92946.
- 30 B. Shen, Y. Li, N. Sun, Y. Zhao and X. Hao, *Nanoscale*, 2020, **12**, 8958–8968.
- 31 M. W. Zhu, Z. J. Wang, Y. N. Chen and Z. D. Zhang, *Surf. Coat. Technol.*, 2013, **216**, 139–144.
- 32 Z. Cao, Z. Wang, N. Yoshikawa and S. Taniguchi, *J. Phys. D: Appl. Phys.*, 2008, **41**, 092003.
- 33 J. Chen, K. R. Udayakumar, K. G. Brooks and L. E. Cross, *J. Appl. Phys.*, 1992, **71**, 4465–4469.
- 34 E. M. Griswold, L. Weaver, M. Sayer and I. D. Calder, *J. Mater. Res.*, 1995, **10**, 3149–3159.
- 35 T. Zhang, W. Li, Y. Zhao, Y. Yu and W. Fei, *Adv. Funct. Mater.*, 2018, **28**, 1706211.
- 36 Y. Z. Li, J. L. Lin, Y. Bai, Y. Li, Z. D. Zhang and Z. J. Wang, *ACS Nano*, 2020, **14**, 6857–6865.
- 37 J. H. Booske, R. F. Cooper, S. A. Freeman, K. I. Rybakov and V. E. Semenov, *Phys. Plasmas*, 1998, **5**, 1664–1670.
- 38 J. Zhai and H. Chen, *Appl. Phys. Lett.*, 2003, **83**, 978–980.
- 39 X. Hao, J. Zhai, F. Shang, J. Zhou and S. An, *J. Appl. Phys.*, 2010, **107**, 116101.
- 40 J. Ge, D. Remiens, J. Costecalde, Y. Chen, X. Dong and G. Wang, *Appl. Phys. Lett.*, 2013, **103**, 162903.
- 41 M. J. Chen, X. K. Ning, S. F. Wang and G. S. Fu, *Nanoscale*, 2019, **11**, 1914–1920.
- 42 X. Guo, J. Ge, F. Ponchel, D. Rémiens, Y. Chen, X. Dong and G. Wang, *Thin Solid Films*, 2017, **632**, 93–96.
- 43 T. Sa, Z. Cao, Y. Wang and H. Zhu, *Appl. Phys. Lett.*, 2014, **105**, 043902.